Supporting materials

Appendix S1

The structure of P(DMDAAC-AM-BA) was shown in Fig. S1. The synthesis method was mentioned in previous work by using Dimethyl diallylammonium chloride (DMDAAC, 60% in aqueous solution), acrylamide (AM), and butyl acrylate (BA) as monomers (Zhang et al., 2010b, a). The employed P(DMDAAC-AM-BA) (100 mg/L in solution) contained 2.0% of BA and 39.2% of DMDAAC. Demulsifier (SD-46) was obtained from the First United Station of Shengtuo in Shengli Oilfield.

The sludge in hydrolysis acidification reactor was originated from the returned sludge of Jinan Refinery and the sludge was cultivated with the mixed solution for 30 d. Mixed solution that feed into hydrolysis acidification reactor was prepared with a ratio of polymer-flooding wastewater and influent of aeration in Jinan Refinery. The sludge that was cultivated in DMBR was also originated from the returned sludge of Jinan Refinery. It was cultivated with the effluent of hydrolysis acidification reactor and the cultivation was conducted for 30 d.

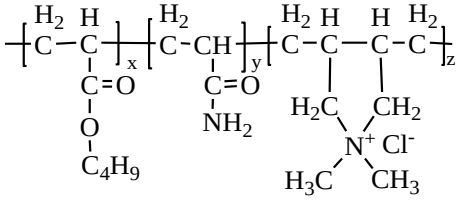

Fig. S1 Structure of P (DMDAAC-AM-BA)

Appendix S2

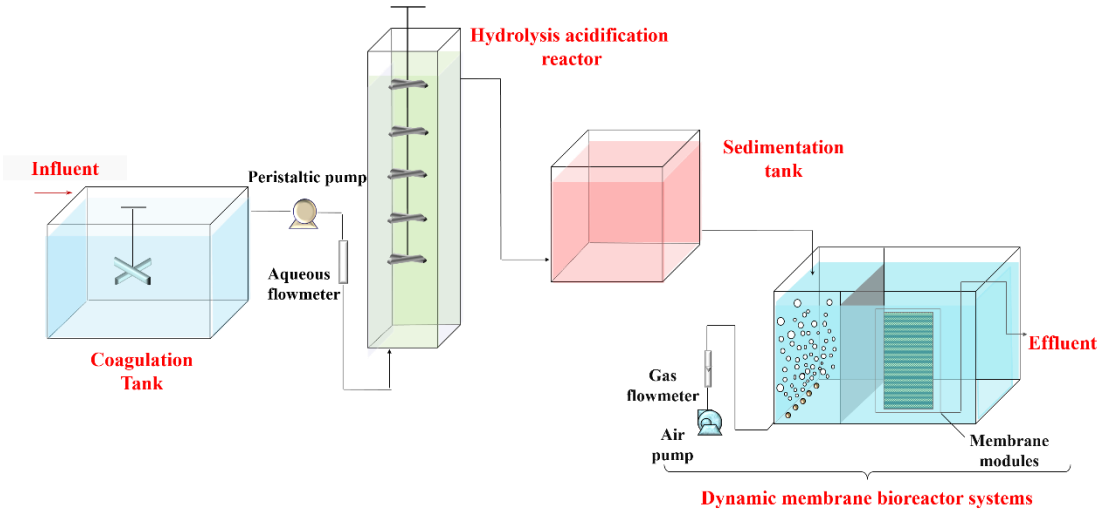

Fig. S2 Schematic illustration of the combined coagulation-hydrolysis acidification-dynamic membrane bioreactor systems

Appendix S3

The fourier transform infrared spectroscopy (FTIR) spectra of the coagulant, P(DMDAAC-AM-BA) were recorded on a FT-IR instrument (Fourier-380 FTIR, USA) with spectra recorded from 4000 to 400 cm^{-1}.

Dynamic light scattering (DLS) results were obtained using a Zetasizer3000Hs (Malvern, UK) at a wavelength of 633 nm. All the measurements were performed at a scattering angle of 90 °in a cell of 4 mm path length at room temperature (25℃ ±1℃).

The transmission electron microscope (TEM) observations of P(DMDAAC-AM-BA) with different contents (0.5%–2.0%) of butylacrylate (BA) were carried out with TEM (Tecnai G2F20 S-TWIN, FEI, Holland).

Appendix S4

FTIR analysis: FT-IR spectra of P(DMDAAC-AM-BA) was given in Fig. S3(a) and the specific FTIR peaks of P(DMDAAC-AM-BA) were presented in Table S1. The characteristic absorption band at 3408.0 cm 1 was assigned to the stretching vibration of -NH2 group in acrylamide (AM). The absorption band at 1654.2 cm^{-1} corresponded well to the amide group stretching vibration in AM. The characteristic absorption band at 2926.6 cm^{-1} was assigned to the -CH_3 connected with -

N^+ in Dimethyl diallylammonium chloride (DMDAAC) (Gao et al., 2014; Lv et al., 2014; Lin et al., 2016). The characteristic absorption peaks at 1455.0 cm^{-1} and 1417.1 cm^{-1} were associated well with the five membered nitrogen containing heterocycles. A sharp peak at 1048.9 cm^{-1} was attributed to the stretching vibration of C-O group in butylacrylate (BA). These results also corresponded to the 1H NMR spectra of P(DMDAAC-AM-BA) (Table S2). Basically, all results mentioned above indicated that the novel coagulant, P(DMDAAC-AM-BA) has been grafted with some functional groups available for coagulating the contaminants from water.

DLS analysis: The size of the aggregation/molecular chain of P(DMDAAC-AM-BA) as well as its aggregation behavior could be evaluated by the DLS analysis. The detected P(DMDAAC-AM-BA) (100 mg/L in solution) contained 2.0% of BA and 39.2% of DMDAAC. Its DLS curve was shown in Fig. S3(b). It was obvious that the particle size distribution of P(DMDAAC-AM-BA) in solution was emerged as bimodal distribution; this was in accordance with the report of Klucker et al. (Klucker et al., 1997). All calculated data were given in Table S3. The peak A was assigned to the single molecule state with average molecule weight of 1.2×10^6. In contrast, peak B represented the multimolecular aggregate and the average molecule weight was about 23.3×10^6. This result indicated that the coagulant, P(DMDAAC-AM-BA) has shown significant intermolecular hydrophobically associating action in water, which would be beneficial to the coagulation behaviors.

TEM analysis: The structure and morphology of the P(DMDAAC-AM-BA) was evaluated by the TEM analysis (Figs. S3(c)–S3(e)). As the hydrophobic monomer (BA) was increased from 0.5% to 2.0%, it was obvious that the structure of P(DMDAAC-AM-BA) was greatly changed and the aggregation of P(DMDAAC-AM-BA) was significantly enlarged. When the hydrophobic monomer content was about 0.5%, the aggregated P(DMDAAC-AM-BA) was distributed only as granular state and no branch structure was observed. The granular state of P(DMDAAC-AM-BA) was increased when the hydrophobic monomer content was increased to 1.0% and in addition, the aggregation of P(DMDAAC-AM-BA) formed a few branches (Fig. S3(d)). As the hydrophobic monomer content was increased to 2.0%, large amounts of branch structures were formed (Fig. S3(e)), which contributed to the aggregation of P(DMDAAC-AM-BA). The more branch structures in P(DMDAAC-AM-BA) would enhance its adsorption bridge capacity, and also the coagulation effect of P(DMDAAC-AM-BA) was greatly improved (Yang et al., 2010).

Basically, all characteristics revealed the large amounts of high-efficiency functional groups and structures available in P(DMDAAC-AM-BA), which would contribute to the coagulation of contaminants from aqueous solution.

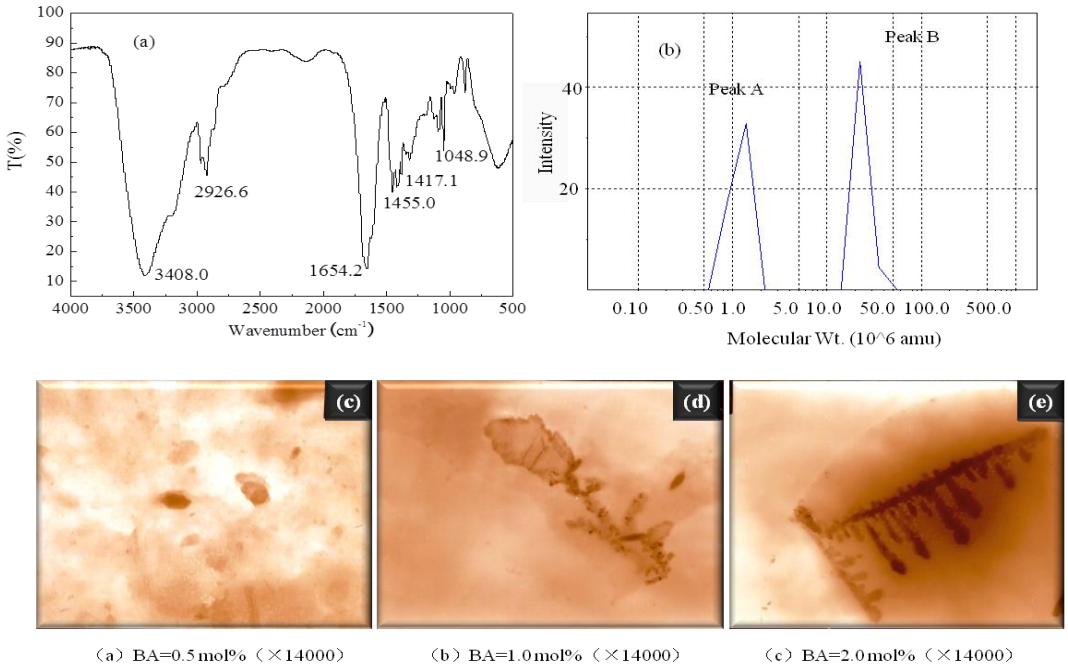

Fig. S3 (a) FT-IR spectra of P(DMDAAC-AM-BA); (b) DLS curve of P(DMDAAC-AM-BA); (c) TEM of P(DMDAAC-AM-BA) with BA = 0.5%; (d) TEM of P(DMDAAC-AM-BA) with BA = 1.0%; (e) TEM of P(DMDAAC-AM-BA) with BA = 2.0%

Table S1 Specific FTIR peaks of P (DMDAAC-AM-BA)

Groups	Wavenumber/cm^{-1}	Units
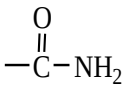	3407.97 1654.17	AM
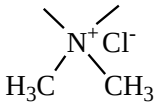	2926.57	DMDAAC
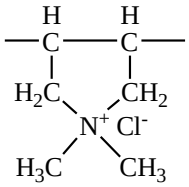	1454.99 1417.05	DMDAAC
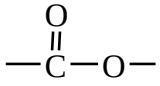	1048.85 1654.17	BA

Table S2 Analysis of ^{1}H-NMR of P(DMDAAC-AM-BA)

Structure	Proton position	Chemical shift
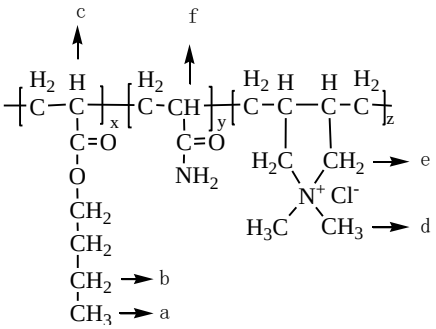	a	1.062–1.097
	b	1.203
	c	2.566
	d	3.135, 3.038,2.919
	e	3.807, 3. 89, 3.691
	f	2.128

Table S3 DLS analysis of P(DMDAAC-AM-BA)

Peaks	Peak width($\times 10^{6}$)	Proportion (%)	Average molecular Wt. ($\times 10^{6}$)
A	0.2	50.3	1.2
B	1.4	49.7	23.3

Appendix S5

Before the coagulation process in combined system, coagulation effect of the novel coagulant, P(DMDAAC-AM-BA), would be evaluated by comparison with other conventional coagulants (APAM, CPAM, EPI-DMA, PAC and $Al_2(SO_4)_3$). Removal of oil and COD by all these coagulants were given in Fig. S4. Results indicated that P(DMDAAC-AM-BA) has exerted the higher capture capacity for oil and COD as compared with other coagulants (APAM, CPAM, EPI-DMA, and PAC). $Al_2(SO_4)_3$ exhibited a similar coagulation effect but its dosage (120 mg/L) was extremely higher than that (10 mg/L) of P(DMDAAC-AM-BA). These results confirmed the improved adsorption bridge capacity of P(DMDAAC-AM-BA). And also, P(DMDAAC-AM-BA) with dosage of 10 mg/L seemed to be suitable for the coagulation process in combined system.

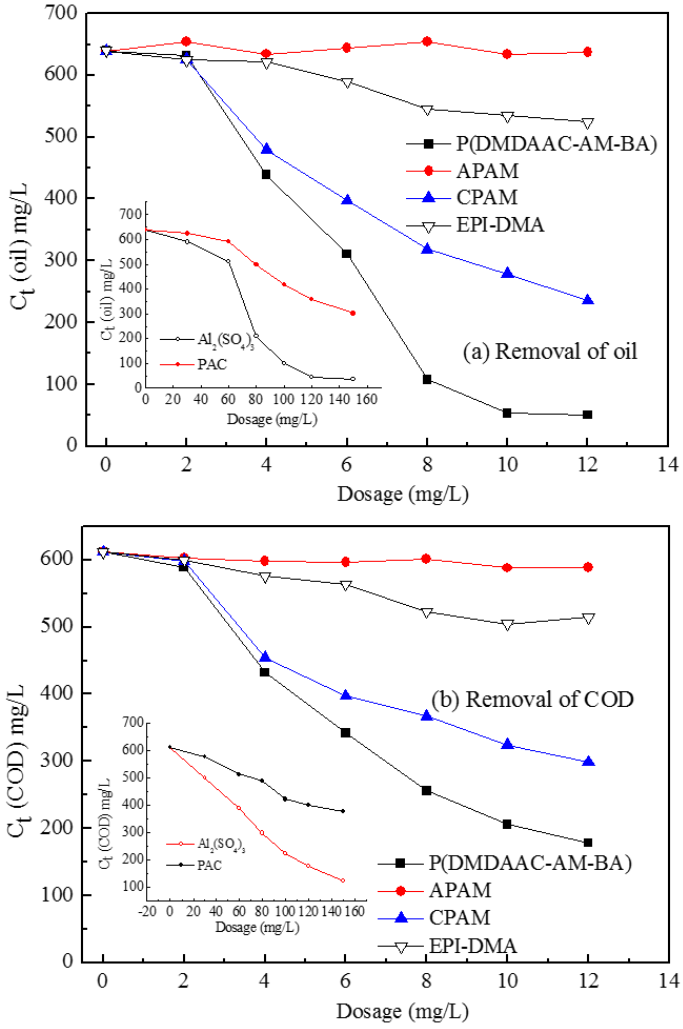

Fig. S4 Coagulation effect of P(DMDAAC-AM-BA) and other conventional coagulants on (a) removal of oil; (b) removal of COD

Appendix S6

To make the mechanism of coagulation process more clear, the coagulation of crude oil was online monitored by photometric dispersion analyzer (PDA). The output signal of PDA was a function of particulate density and particle size in water, which could intuitively reflect the aggregation state of particles. As a result, the output signal of PDA was also called as flocculation index (FI) (Järnström et al., 1995a; Järnström et al., 1995b; Li et al., 2007). The FI in coagulation process was automatically recorded and was used in subsequent analysis of characteristic parameters.

After adding P(DMDAAC-AM-BA) - demulsifier (SD-46), the solution was stirred rapidly at 200 r/min for 2 min. It was followed by the slow stirring (40 r/min) until the curve of FI reaching the first plateau and then the slow stirring was kept for 2 min. To evaluate the strength of formed

floc, the solution was then stirred strongly (400 r/min) for 1.5 min, and reinstated the slow stirring (40 r/min) until the curve of FI reaching the second plateau. The typical curve of FI was shown in Fig. S5. A control test without demulsifier (SD-46) added was also conducted according to the procedures mentioned above so as to consider the flocculation index of P(DMDAAC-AM-BA).

The characteristic parameters that could be obtained from the curve of FI included: slope, h_0, h_1, h_2, h_3, t_1, and t_2 (Fig. S5). The slope was the maximum rate of FI curve in ascent stage, representing the flocculation rate. The h_0 was the initial value of FI. The h_1, h_2 and h_3 represented the average size of floc obtained at first plateau, average size of the smallest floc during the strong stirring and average size of floc obtained at second plateau. The t_1 represented the time when the floc began to form and the t_2 mean the time for appearance of the vertex of FI curve.

The floc strength was represented by the "strength factor" *S* and the equation was given as Eq. (S1):

$$S = \frac{h_2}{h_1} \times 100\%, \qquad \text{(S1)}$$

The floc recovery was represented by the "recovery factor" *R* and the equation was given as Eq. (S2):

$$R = \frac{h_3 - h_2}{h_1 - h_2} \times 100\%, \qquad \text{(S2)}$$

The characteristic parameters of FI curve after adding of P(DMDAAC-AM-BA) and P(DMDAAC-AM-BA) - demulsifier (SD-46) were given in Table S4. As shown in Table S2, the slope (71.8×10^{-4}) of FI after adding of P(DMDAAC-AM-BA) was higher than that (59.5×10^{-4}) of P(DMDAAC-AM-BA) - demulsifier (SD-46); this result corresponded well to the t_1, and t_2. The vertex of FI curve obtained from P(DMDAAC-AM-BA) was about 139 s. In contrast, vertex of FI for P(DMDAAC-AM-BA) - demulsifier (SD-46) required about 253 s. These results indicated that the coagulant, P(DMDAAC-AM-BA), could achieve higher flocculation rate and floc size at first plateau due to its quick and efficient bridging flocculation mechanism. However, the strength of floc (*S* %) obtained from P(DMDAAC-AM-BA) was too low (with only 15%) as compared with that (60%) obtained from P(DMDAAC-AM-BA) - demulsifier (SD-46). This result illustrated that the using of P(DMDAAC-AM-BA) alone could not ensure the stability of floc during the coagulation process, and the added demulsifier (SD-46) could improve the floc strength by destroying the interfacial film between the crude oil particles. Under this condition, the size of floc obtained at second plateau (h_3) followed the reverse order as: P(DMDAAC-AM-BA)-demulsifier (SD-46) > P(DMDAAC-AM-BA); this was in accordance with the size distribution of oil in coagulation process.

As all mentioned above, a potential mechanism of the oil coagulation by P(DMDAAC-AM-BA)-demulsifier (SD-46) could be concluded as three steps and it was given in Fig. S6. In the step (A), the scattered oil particles in aqueous solution could be aggregated by the coagulant, P(DMDAAC-AM-BA), through bridging flocculation and electrostatic interaction. The collisions of aggregated oil occurred on the P(DMDAAC-AM-BA) chains partially due to the chain contortion and rotation of this high-molecular coagulant in the step (B). These collisions would induce two or more oil

particles into one big particle when the interfacial film between the oil particles was destructed by the demulsifier in step (C). During this process, the size of floc as well as the floc strength was greatly reinforced, which resulted in a high coagulating effect on the crude oil.

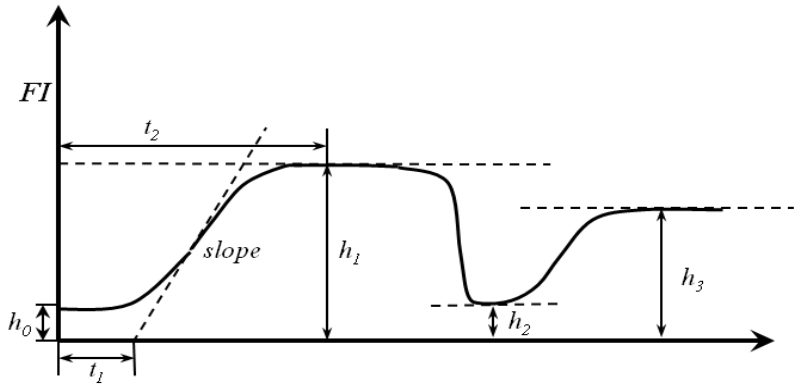

Fig. S5 Typical curve of flocculation index (FI)

Table S4 Characteristic parameters obtained from FI curve after adding P(DMDAAC-AM-BA)- demulsifier (SD-46) and P(DMDAAC-AM-BA)

Parameters	slope($\times 10^{-4}$)	h_1	h_2	h_3	S(%)	R(%)	t_1(s)	t_2(s)
P(DMDAAC-AM-BA)	71.8	0.53	0.08	0.26	15	40	19	139
P(DMDAAC-AM-BA)-demulsifier	59.5	0.42	0.25	0.33	60	47	22	253

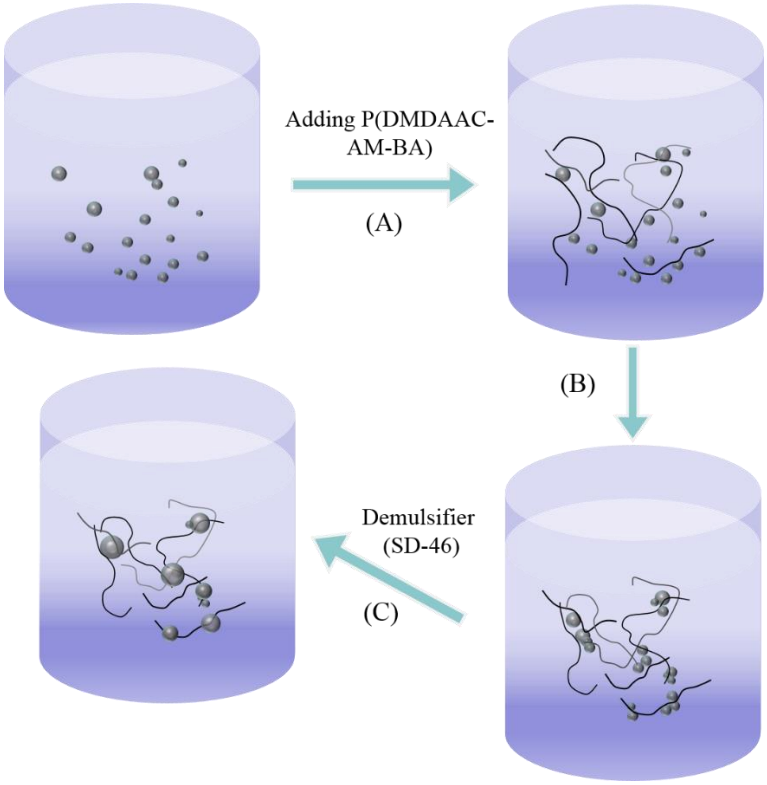

Fig. S6 A potential mechanism of the oil coagulation by P(DMDAAC-AM-BA)-demulsifier (SD-46)

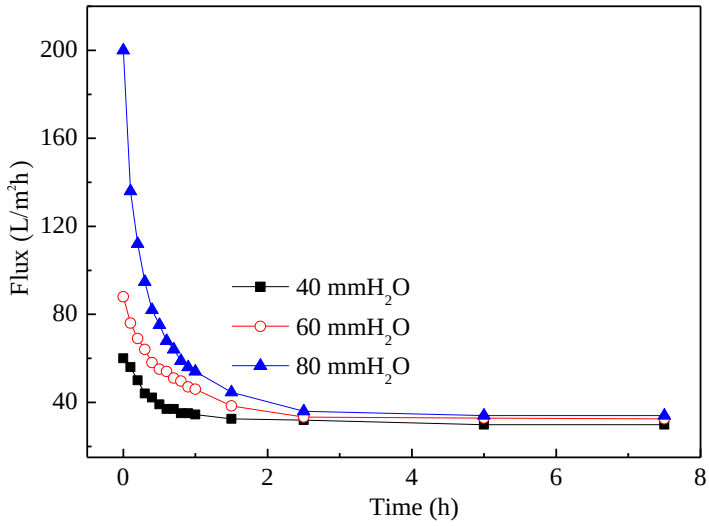

Fig. S7 Permeate flux change at different constant-pressure operating conditions

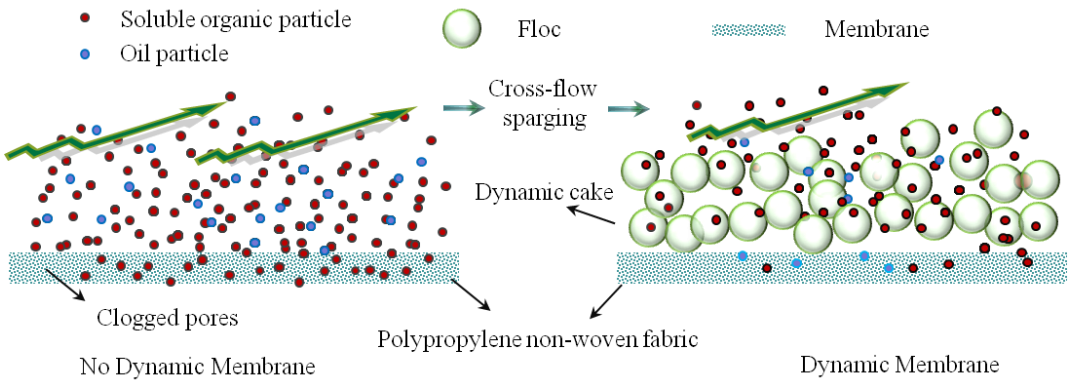

Fig. S8 Scheme of the dynamic membrane formation

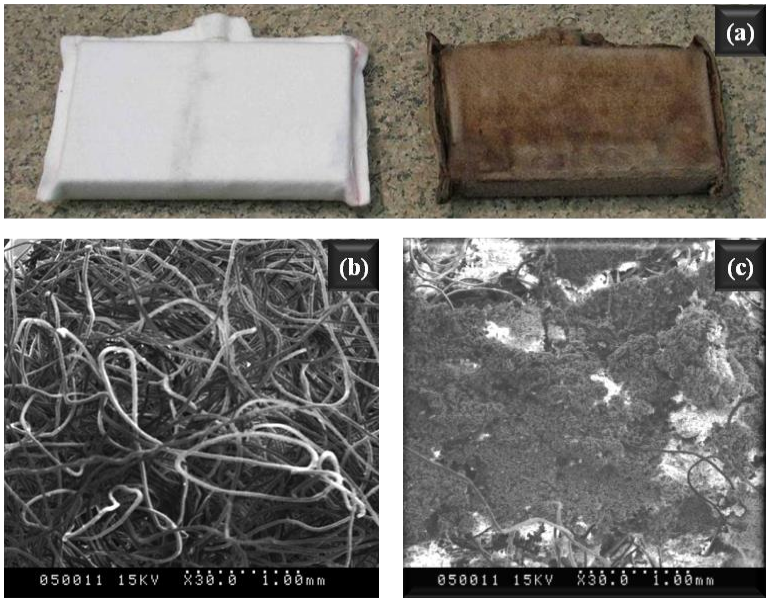

Fig. S9 Appearance of membrane module before and after use (a); SEM of membrane module before use (b); SEM of membrane module after use (c)

References

Gao D, Chen C, Ma J, Duan X, Zhang J (2014). Preparation, characterization and antibacterial functionalization of cotton fabric using dimethyl diallyl ammonium chloride-allyl glycidyl ether-methacrylic/nano-ZnO composite. Chemical Engineering Journal, 258(15): 85–92

Järnström L, Lason L, Rigdahl M (1995a). Flocculation in kaolin suspensions induced by modified starches 1. Cationically modified starch—effects of temperature and ionic strength. Colloids and Surfaces. A, Physicochemical and Engineering Aspects, 104(2–3): 191–205

Järnström L, Lason L, Rigdahl M, Eriksson U (1995b). Flocculation in kaolin suspensions induced by modified starches 2. Oxidized and hydrophobically modified oxidized starch in comparison with poly(vinyl alcohol) and carboxymethylcellulose. Colloids and Surfaces. A, Physicochemical and Engineering Aspects, 104(2–3): 207–216

Klucker R, Munch J P, Schosseler F (1997). Combined static and dynamic light scattering study of associating random block copolymers in solution. Macromolecules, 30(13): 3839–3848

Li T, Zhu Z, Wang D, Yao C, Tang H (2007). The strength and fractal dimension characteristics of alum–kaolin flocs. International Journal of Mineral Processing, 82(1): 23–29

Lin Q, Gao M, Chang J, Ma H (2016). Adsorption properties of crosslinking carboxymethyl cellulose grafting dimethyldiallylammonium chloride for cationic and anionic dyes. Carbohydrate Polymers, 151(20): 283–294

Lv S, Sun T, Zhou Q, Liu J, Ding H (2014). Synthesis of starch-g-p(DMDAAC) using HRP initiation and the correlation of its structure and sludge dewaterability. Carbohydrate Polymers, 103(15): 285–293

Yang Z L, Gao B Y, Li C X, Yue Q Y, Liu B (2010). Synthesis and characterization of hydrophobically associating cationic polyacrylamide. Chemical Engineering Journal, 161(1–2): 27–33

Zhang Y, Gao B, Lu L, Yue Q, Wang Q, Jia Y (2010a). Treatment of produced water from polymer flooding in oil production by the combined method of hydrolysis acidification-dynamic membrane bioreactor–coagulation process. Journal of Petroleum Science Engineering, 74(1–2): 14–19

Zhang Y, Gao B, Lu L, Yue Q, Wang Q, Jia Y (2010b). Treatment of produced water from polymer flooding in oil production by the combined method of hydrolysis acidification-dynamic membrane bioreactor–coagulation process. Journal of Petroleum Science Engineering, 74(1–2): 14–19